Characterization of 14 Karat Gold Alloys

Abstract

This paper is a continuation of the project we presented at the 2010 Santa Fe Symposium® in which we defined a characterization system and analysis of data on 18K gold alloys. The research carried out since then has enabled us to connect the physical-mechanical characteristics of each alloy with its chemical composition, thereby identifying the best solution possible to produce a specific item. We have decided to report all data related to the analysis of 14K white- and colored-gold alloys, including alloys suitable for both investment casting and fabrication. We used the same characterization method presented in our 2010 paper, so it will not be specified once again.

Data Analysis

Fourteen-karat colored-gold alloys have been divided into yellow- and red-gold alloys. We decided to adopt this distinction because of the large number of redgold alloys at our disposal and to carry out more extensive analysis. Since all testing was carried out only on 14K alloys, from now on we will omit specifying we are talking about 14K gold alloys.
Thirty-two yellow-gold alloys were analyzed and are in Table 1. These alloys were sorted in increasing order based on silver and zinc concentrations. We also highlighted any presence of grain refiners or deoxidizers for each alloy.

Table 1 Composition of the 14K investigated yellow gold alloys (weight %)

Specimen	Au	Ag	Zn	Cu	GR1	GR2	Deoxidizers
Alloy 1	585	20.75	41.5	Balance	X		
Alloy 2	585	20.75	58.1	Balance	X		
Alloy 3	585	20.75	66.4	Balance	X		
Alloy 4	585	20.75	95.45	Balance		X	
Alloy 5	585	20.75	95.45	Balance	X		
Alloy 6	585	20.75	95.45	Balance			X
Alloy 7	585	41.5	58.1	Balance		X	
Alloy 8	585	41.5	70.55	Balance			X
Alloy 9	585	41.5	83	Balance	X		
Alloy 10	585	41.5	95.45	Balance			X
Alloy 11	585	51.875	56.025	Balance			X
Alloy 12	585	53.95	95.45	Balance		X	
Alloy 13	585	62.25	62.25	Balance	X		
Alloy 14	585	62.25	62.25	Balance			X
Alloy 15	585	83	41.5	Balance	X		
Lega 16	585	83	62,25	Balance	X		
Lega 17	585	83	66.4	Balance			X
Lega 18	585	95,45	37,35	Balance			X
Lega 19	585	95,45	53,95	Balance			X
Lega 20	585	101,675	66.4	Balance	X		
Lega 21	585	103,75	83	Balance			X
Lega 22	585	119,935	39,965	Balance		X	
Lega 23	585	124,5	103,75	Balance	X		
Lega 24	585	124,5	103,75	Balance			X
Lega 25	585	128,65	43,575	Balance	X		
Lega 26	585	130,725	42,745	Balance			X
Lega 27	585	186,75	41,5	Balance	X		
Lega 28	585	195,05	8,3	Balance	X		
Lega 29	585	228,25	29,05	Balance	X		
Lega 30	585	234,475	14,525	Balance	X		
Lega 31	585	257,3	6,225	Balance	X		
Lega 32	585	265,6	14,525	Balance	X		

First of all, we highlighted solidus and liquidus temperature values, which are symbolized by a square and a triangle, of all alloys in Table 1. We carried out a first interpolation with all values, which resulted in the graph in Figure 1.

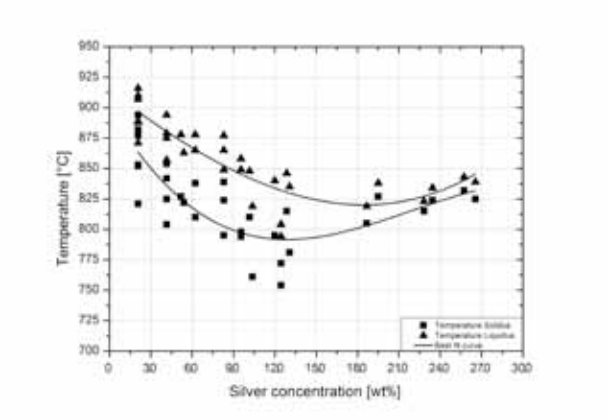

Figure 1 Graph of liquidus and solidus temperatures (°C) against silver concentration (wt.%)

We then decided to get interpolation curves excluding liquidus and solidus temperature values of alloys with a zinc content above 8.0%, i.e., alloys 4, 5, 6, 9, 10, 12, 21, 23, 24. Best fit curves were determined on twenty-three values and can be seen in Figure 2.

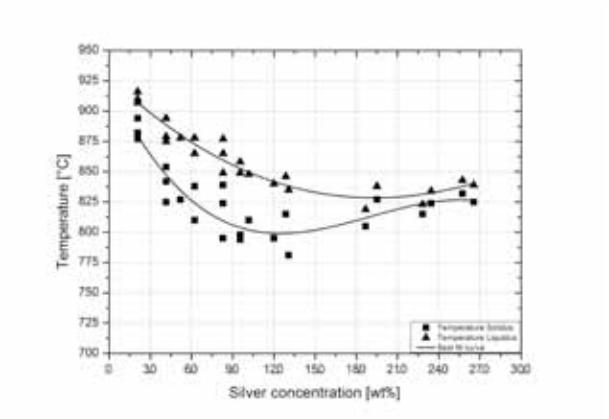

Figure 2 Graph of liquidus and solidus temperatures (°C) against silver concentration (wt.%), excluding alloys with zinc concentration above 8.0%

Analyzing changes in experimental data based on silver content, we see that by increasing the silver content, both solidus and liquidus temperatures initially decrease, then they enter a second stage where they increase. The difference between the interpolated solidus and liquidus values decreases with the addition of silver, showing an opposite behavior compared to that seen with 18K alloys. This can be linked to the fact that with 14K alloys, an increase in silver content means a decrease in zinc. The wide melting range could be influenced by the zinc concentration (which on average is greater for alloys with less silver content).

The graph of Figure 3 shows density variation based on silver content. It shows that an increase in silver causes an increase in density. The influence of zinc on density can be observed with alloys 1, 2, 3 and 4 in which, silver concentration being equal, zinc increases from alloy 1 to alloy 4. The result is that, with an equal content of silver, an increase of zinc means a decrease in density.

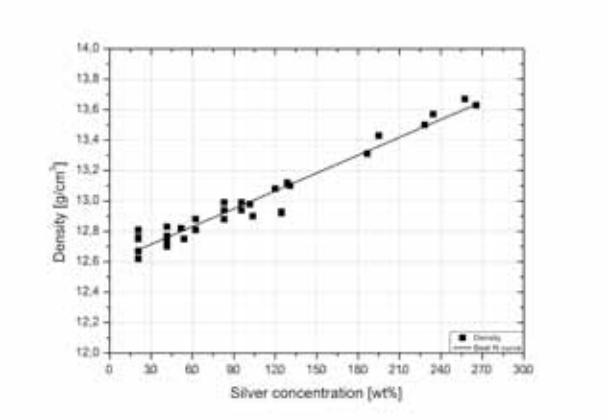

Figure 3 Graph of the density (g/cm^3) against silver concentration (wt.%)

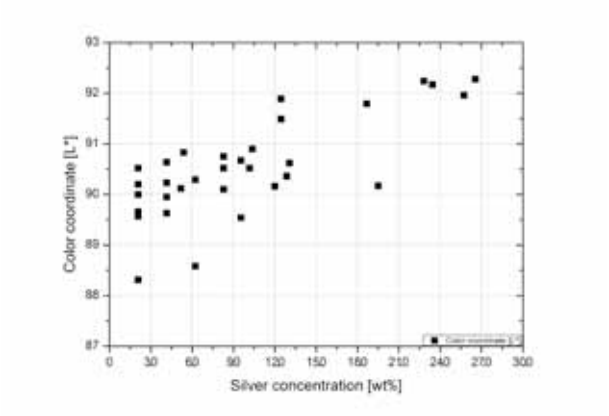

Figure 4 Graph of L* against silver concentration (wt.%)

Analyzing L* color coordinate changes in Figure 4, there is a general increase with silver content. It appears that, silver being equal, an increase in zinc is followed by an L* value increase (little information is available in this respect). On the other hand, no law seems to explain this phenomenon. For this reason we decided to analyze L* progress based on the sum of silver and double the content of zinc.
This way we achieved a more defined trend (Figure 5) but still not acceptable in our view because some data are still too far from the interpolation curve (e.g., alloy 13 diverges a lot from the best-fit curve).

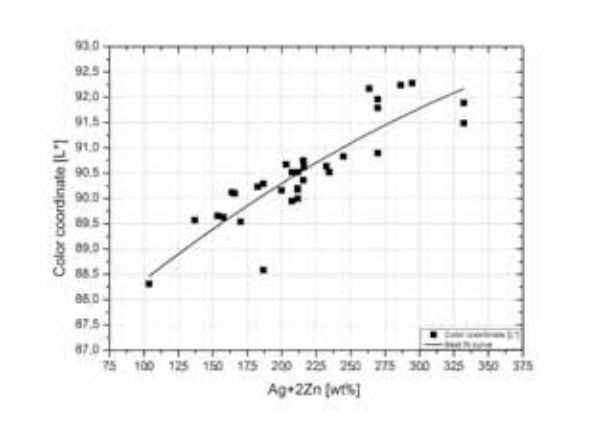

Figure 5 Graph of L* against silver and double the zinc concentration (wt.%)

In a* color coordinate, an increase of silver makes the color change from red to green. In Figure 6 we considered a* progress depending on the sum of silver and double the zinc concentration. This decision was made because zinc seems to influence the change of color toward green more than silver. After analyzing all alloys we can affirm that the resulting interpolation is good and allows us to confirm that the influence of zinc in changing color toward green is double compared to silver.

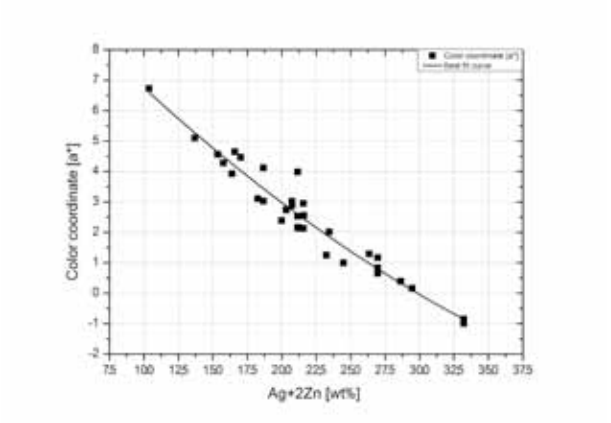

Figure 6 Graph of a* against silver and double zinc concentration (wt.%)

Looking at the b* color coordinate, in which "color dimension" changes from blue to yellow, we see a rising trend depending on silver and zinc content with a consequent shift towards yellow (Figure 7). Comparing alloys 21, 27, 30 and 31, we see that by increasing zinc concentration there is a gradual shift of the b* color coordinate toward blue. The interpolation curve was achieved by excluding data on alloys 23 and 24, which were too far from the other dots (we are referring to the two dots on the right of the graph, much lower than all the other data). The reason is because alloys 23 and 24 have a higher zinc concentration, and this probably strongly influences final experimental results.

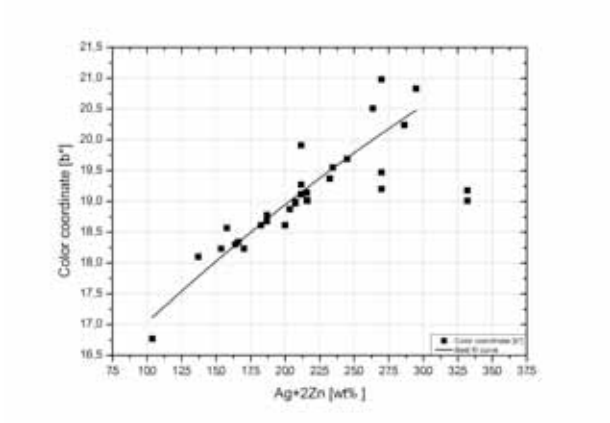

Figure 7 Graph of b* against silver and double the zinc concentration (wt.%)

Let's proceed by analyzing the registered hardness trend. Figure 8 shows that hardness changes after solution annealing and after precipitation hardening, both of which show significant trends as we already explained in our 2010 Santa Fe Symposium® paper. Hardness after casting, on the contrary, could be influenced by cooling conditions.

The graph highlights how an increase in silver concentration increases hardness (which is exactly the opposite for 18K), both for solution-annealed and precipitation-hardened specimens. The square symbol represents hardness after solution annealing and the triangle refers to hardness after hardening heat treatment. (We have reported the maximum hardness value recorded irrespective of temperature and time necessary to reach that specific value.) Our results clearly indicate that silver is the element that affects the matching hardness the most. This leads us to think hardness happens through precipitation in a second stage, which is silver-rich, and not in order and disorder as with 18K alloys. With an equal content of silver, alloys with more zinc seem to have slightly lower hardness values. It is still to be seen whether zinc can influence maximum reachable hardness values by changing temperature and time. Based on our data it seems that, silver being equal, an alloy with more zinc can reach maximum hardness values by staying in the furnace a shorter time. The graph in Figure 8 seems to indicate that in order for an alloy to be hardened (with proper heat treatment), it must have at least 7.5% silver.

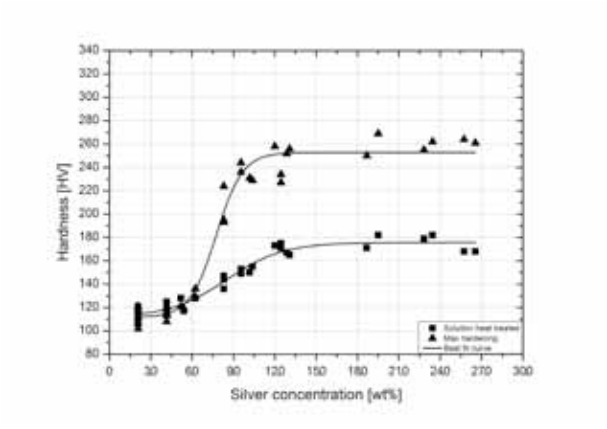

Figure 8 Graph of hardness against silver concentration (wt.%)

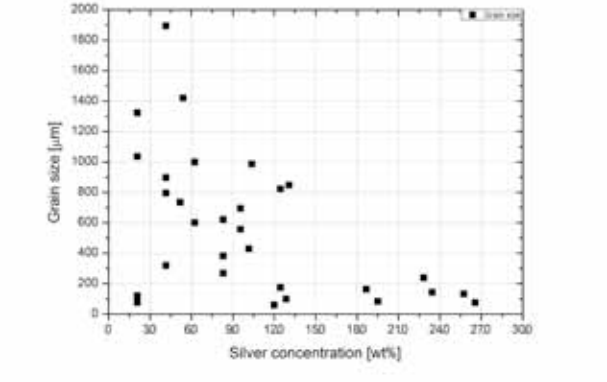

Figure 9 Graph of average grain size against the silver concentration (wt.%)

With reference to grain size in the graph in Figure 9, it is not possible to extrapolate a trend based on silver concentration. We can only say that alloys with grain refiner 1 (GR1) are on average well refined whereas alloys with grain refiner 2 (GR2) clearly show larger grains (they should be considered non-grain-refined alloys). Alloys with deoxidizer, on the other hand, clearly have the largest grains.

Observation carried out with 14K confirmed what was observed with 18K. In this case as well, grain refiner 2 is cobalt and we believe that, as for 18K, this element should be considered a solid-phase grain refiner, i.e., it can produce relatively small grains only during annealing.

Before analyzing 14K red-gold alloys we separately took into consideration all data about alloys for investment casting and alloys suitable for deformation.

14K Yellow-Gold Alloys for Investment Casting

Eleven 14K alloys were suitable for investment casting, i.e., alloys 6, 8, 10, 11, 14, 17, 18, 19, 21, 24, and 26. Different from 18K, we decided to consider alloys with at least one deoxidizer as suitable for investment casting because the high amount of zinc in 14K could cause surface defects. We also believe that alloys with little zinc (with no deoxidizer) could be considered suitable for investment casting, such as alloys 28 or 31, but for investment casting we prefer to consider and suggest only 14K alloys with deoxidizer. After casting, ultimate tensile stress (UTS) and yield strength (YS) show a rising trend following an increase in silver concentration (Figure 10).

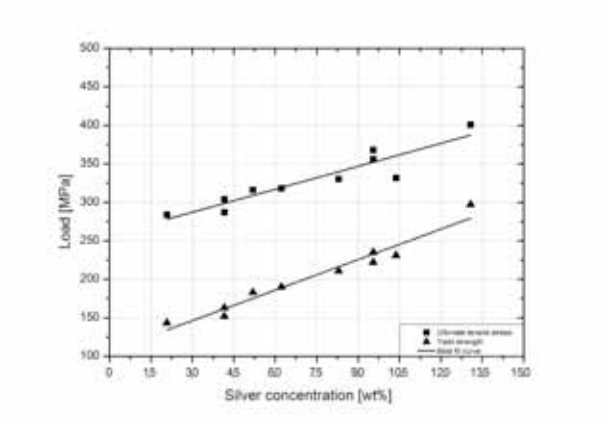

Figure 10 Graph of UTS and YS (after casting) against silver concentration (wt.%)

We can generally affirm that tensile strength increases by increasing silver. The divergence of some data is due to the high content of zinc. For example, alloy 24 has the highest zinc content and displays the most divergence from the calculated best-fit curve. It seems that increases of zinc are followed by a reduction of ultimate tensile stress and yield strength.

We would like to stress that, with reference to deoxidized alloys, it is possible to reach a maximum silver concentration around 13%. There is almost no alternative to this choice because silicon is the most used deoxidizing element, and it has little solubility in gold-silver systems. It tends to concentrate on the grain boundaries, constituting low-melting phase compounds causing embrittlement. For this reason you cannot have silver content higher than 13% when silicon is present.

As far as after-casting elongation is concerned, there is a decreasing trend with silver content. In this case an increase in silver reduces elongation, in line with what we observed with tensile and yield strength, i.e., greater UTS and YS see minor elongations. In the following graph (Figure 11), we considered only alloys with silicon (alloys 6, 8,

10, 11, 14, 17, 18, 19, 21, 24, and 26).

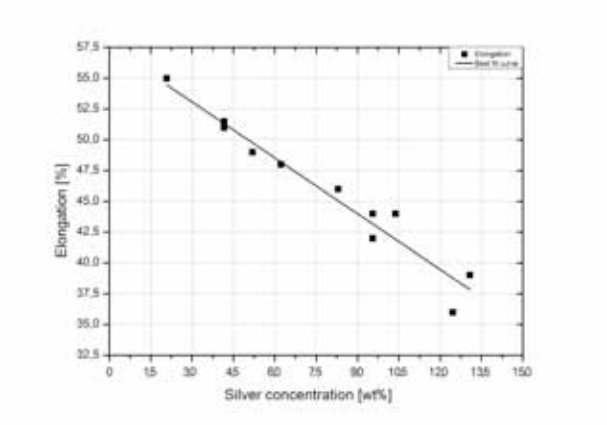

Figure 11 Graph of percent elongation to rupture against silver concentration (wt.%)

Wrought 14K Yellow-Gold Alloys

Twenty-one 14K alloys are suitable for plastic deformation (alloys 1, 2, 3, 4, 5, 7, 9, 12, 13, 15, 16, 20, 22, 23, 25, 27, 28, 29, 30, 31, and 32). In this case we considered only alloys with at least one grain refiner. We measured mechanical characteristics, drawability and work hardening curves. With reference to tensile and yield strength following annealing, results are shown in the graph in Figure 12. In this case, as well, we would like to stress that both the tensile and yield strength are increased with greater silver concentration in the alloy. The graph features several experimental dots that diverge from the interpolated line. These can be caused by several factors linked to the chemical composition of each alloy but, foremost, it depends on the zinc concentration. We believe that a higher zinc content causes lower tensile and yield strength. Alloys with grain refiner 1 show greater tensile and yield strength compared to alloys with grain refiner 2.

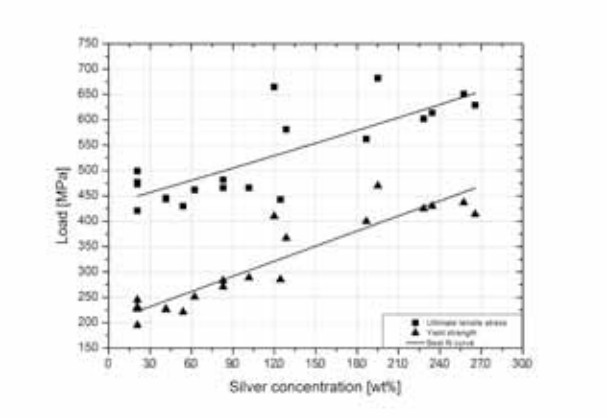

Figure 12 Graph of UTS and YS against silver concentration (wt.%)

The deformation trend after annealing (Figure 13) shows a decrease when silver concentration increases. Please note that alloys with low tensile strength show high deformation, as expected. An increase in zinc is followed by greater elongation. Tensile and yield strengths are clearly higher in the wrought alloys compared to investment casting alloys, which only have the deoxidizer, whereas elongation is less (see graphs in Figures 10 and 12 and in Figures 11 and 13).

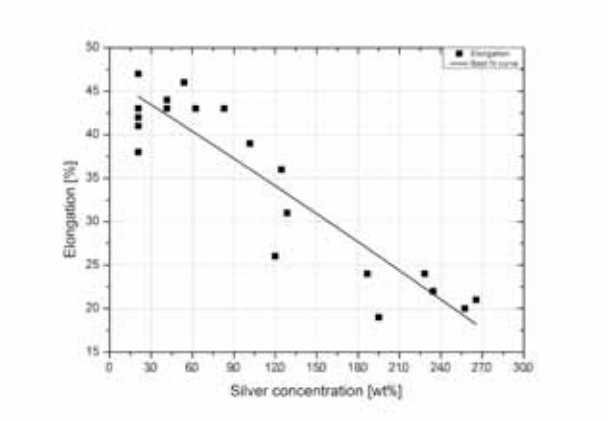

Figure 13 Graph of percent elongation to rupture against silver concentration (wt.%)

Drawability values in Figure 14 are greatly affected by silver and zinc content.
More specifically, in the following graph we see a decreasing trend in drawability when the silver concentration increases whereas, silver being equal, an increase of zinc causes drawability to increase. Another parameter which influences this property is grain size. Silver and zinc content being equal (alloys 4, 5 and 6), the bigger the grain size, the greater the drawability is. In the interpolation of the graph in Figure 14, we did not consider values of alloys with grain refiner 2 (alloys 4, 7, 12 and 22 – the stars in the graph).

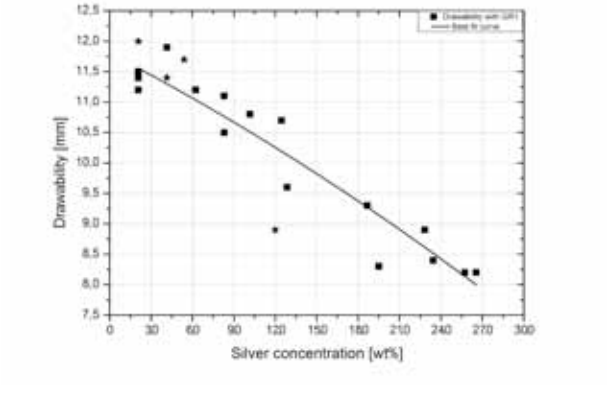

Figure 14 Graph of drawability against silver concentration (wt.%)

The graph in Figure 15 features work-hardening values of just some alloys (alloys 1, 13, 16, 20, 25,

28, 30, and 32), each featuring a different content of silver. By analyzing work-hardening curves we can affirm that materials tend to work harden more with increasing silver content.

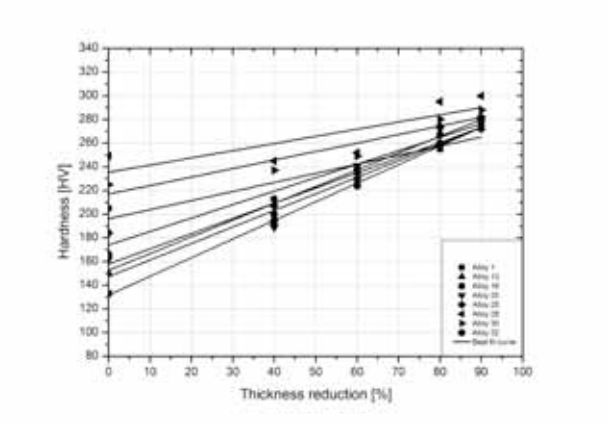

Figure 15 Work hardening best-fit curves for 14K yellow-gold alloys

14K Red-Gold Alloys

Table 2 features 18 red-gold alloys. These alloys were sorted by increasing order of silver and zinc concentration.

Table 2 Composition of the investigated 14K red-gold alloys (weight %)

Specimen	Au	Ag	Zn	Cu	GR1	GR2	Deoxidizers
Alloy 1	585	6.225	6.225	Balance		X	
Alloy 2	585	6.225	6.308	Balance			X
Alloy 3	585	10	15	Balance	X		
Alloy 4	585	14.525	14.525	Balance		X	
Alloy 5	585	16.6	12.45	Balance	X		
Alloy 6	585	41.5	8.3	Balance		X	
Alloy 7	585	41.5	12.45	Balance	X		
Alloy 8	585	45.65	24.9	Balance	X		
Alloy 9	585	50	15	Balance	X		X
Alloy 10	585	52	5	Balance	X		X
Alloy 11	585	56.025	20.75	Balance			X
Alloy 12	585	70.55	18.675	Balance		X	
Alloy 13	585	74.7	4.15	Balance		X	
Alloy 14	585	74.7	4.15	Balance	X		
Alloy 15	585	74.7	4.15	Balance	X		
Alloy 16	585	83	20.75	Balance	X		
Alloy 17	585	120.35	12.45	Balance			X
Alloy 18	585	132.8	8.3	Balance	X		

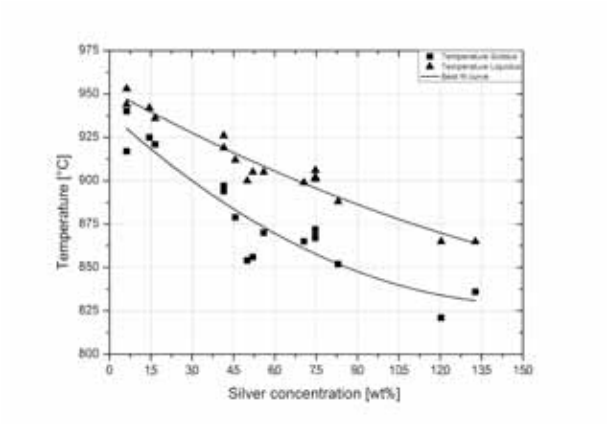

Figure 16 Graph of liquidus and solidus temperatures (°C) against silver concentration (wt.%)

Both the solidus and liquidus temperatures decrease progressively as the silver content is increased in 14K red-gold alloys as opposed to yellow-gold alloys. However, the decreasing trend for solidus is more marked. With more silver, the difference between liquidus and solidus is greater (alloy melting range increases).

Density increases as the silver content is increased in 14K red-gold alloys, as is observed in yellow-gold alloys. No specific remarks can be made about the influence of zinc in this regard because of the small number of alloys analyzed and the variation in zinc content (please note that we are talking about a maximum density variation in the range of 0.5 g/cm3). Interpolation was carried out without considering alloys 12 and 15, which greatly diverged from the other results, as seen in Figure 17 (the two stars).

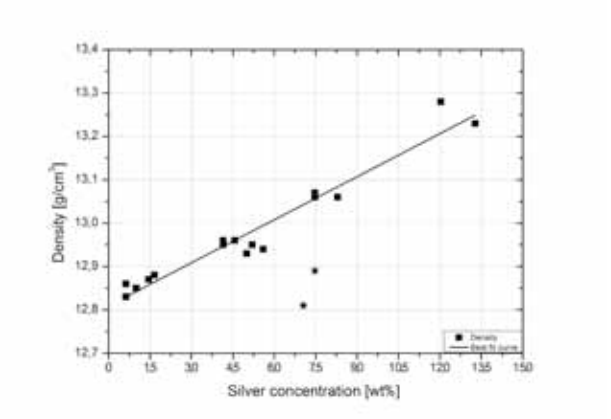

Figure 17 Graph of the density (g/cm³) against silver concentration (wt.%) in red-gold alloys

Looking at L* color coordinate, no trend regarding silver concentration could be interpolated (Figure 18). We can only affirm that by increasing silver the L* value increases, but we are not able to say according to what law. Even considering the "double effect" of zinc, a reasonable curve cannot be achieved. In any case, in Figure 19 we tried to mark an increase in L* depending on silver and double the zinc.

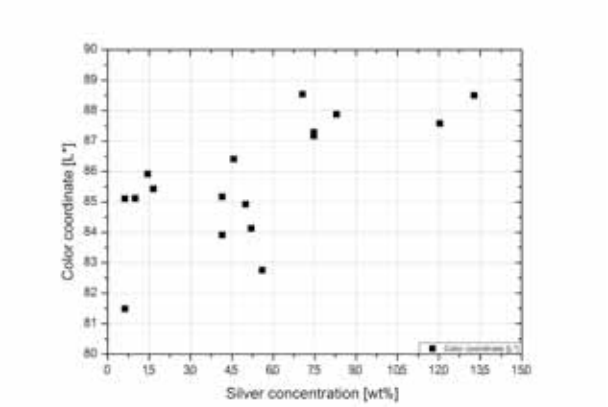

Figure 18 Graph of L* against silver concentration (wt.%)

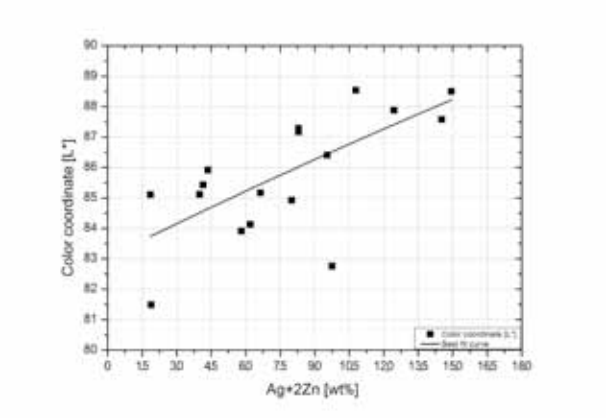

Figure 19 Graph of L* against silver and double zinc concentration (wt.%)

With color coordinates a* and b*, considering the trend based on the sum of silver and double the zinc, we managed to get fairly reasonable trends. As expected for a*, increasing the content of silver and zinc changes the color towards green (less red), and zinc has double the effect compared to silver (content being equal). The b* value shifts towards yellow when silver and zinc increase.

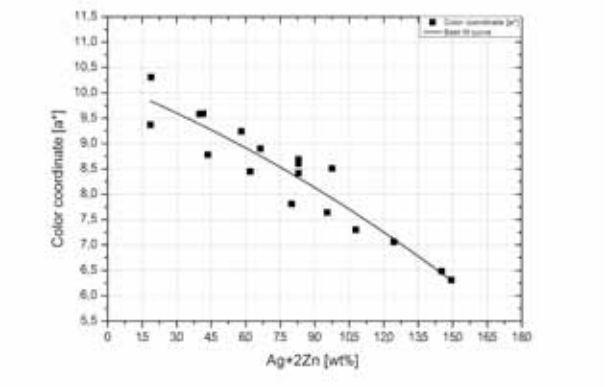

Figure 20 Graph of a* against silver and double zinc concentration (wt.%)

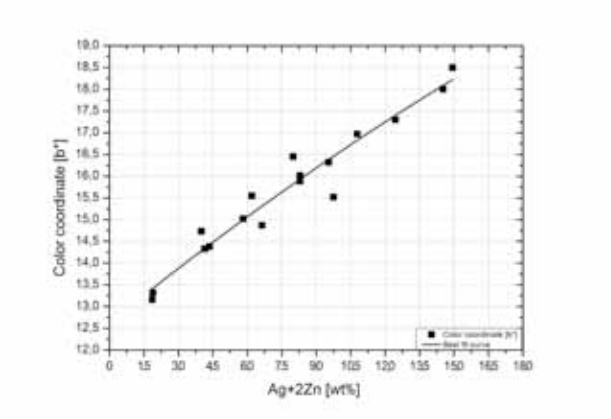

Figure 21 Graph of b* against silver and double zinc concentration (wt.%)

With reference to hardness, we believe the same considerations stated for yellow gold still apply. Hardness tends to increase with silver concentration, as seen in Figure 22. Please note that for alloys with less than 6.0% silver, there is no difference between hardness before and after precipitation hardening. In this case the minimum concentration for an acceptable hardness increase following heat treatment is fixed at 7.5%. Therefore, in this case hardness is through precipitation and is not influenced by possible gold-copper order.

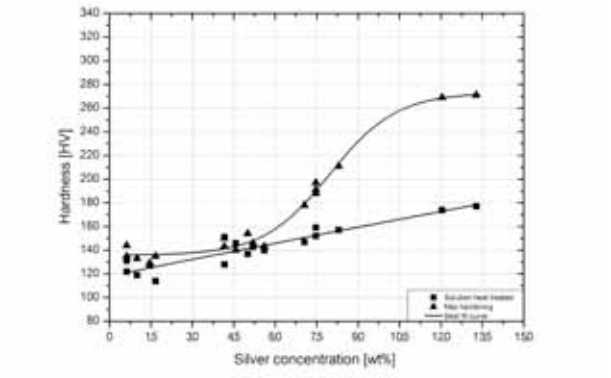

Figure 22 Graph of hardness against silver concentration (wt.%)

14K Red-Gold Alloys for Investment Casting

Twelve 14K alloys were suitable for investment casting (alloys 2, 3, 5, 7, 9, 10, 11, 14, 15, 16, 17, and 18). With reference to 14K red-gold investment casting alloys, we considered only alloys with at least one deoxidizer or grain refiner 1 and zinc content less than 2.1% (alloy 8 is therefore excluded).

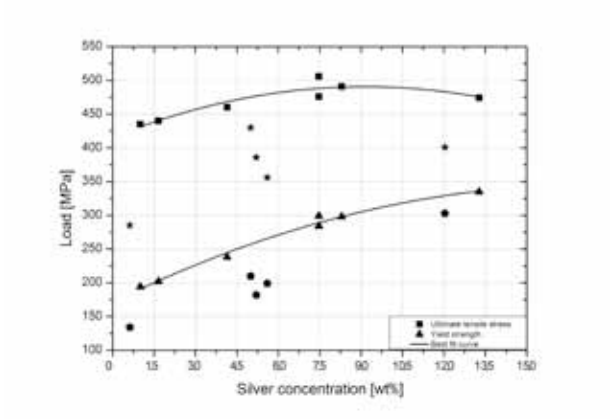

Figure 23 Graph of UTS and YS against silver concentration (wt.%)

The graph in Figure 23 highlights how UTS and yield strength tend to increase with silver concentration. It appears yield strength is more influenced by silver concentration than UTS. Trends were calculated without considering alloys with deoxidizer, which are represented by stars and pentagons (alloys 2, 9, 10, 11, 17). We did not manage to calculate a trend even considering all investment casting alloys, thereby confirming how much the deoxidizer influences mechanical properties of the examined alloys. Based on the same graph, it should be noted that with reference to yield strength, alloys with deoxidizer have a trend similar to alloys with only grain refiner, i.e., a similar trend could be calculated for alloys with grain refiner only. With reference to UTS as well, we can affirm that its trend is similar to that of alloys with grain refiner only. The two stars that diverge the most refer to alloys 9 and 10, which contain a grain refiner as well as a deoxidizer. They seem to increase UTS more than YS and do not follow the trend exhibited by alloys with only a deoxidizer. To summarize, we believe the deoxidizer reduces the mechanical properties of the alloys but that trend depends on silver content and is more or less the same as for alloys with a grain refiner. We could also say that the deoxidizer reduces tensile strength more than yield strength.

The graph in Figure 24 shows the trend of elongation without considering alloys 2, 9, 10, 11, 17 (represented by stars), namely alloys with deoxidizer. It should be noted that elongation decreases when silver concentration increases (in accordance with the growth of mechanical properties observed in Figure 23). In the case of elongation we believe the previous considerations on the deoxidizer still apply, i.e., that generally speaking elongation is decreased depending on silver, and alloys 9 and 10 do not reflect this trend because they are grain-refined. The elongation of deoxidized alloys is inferior to that of grain-refined alloys.

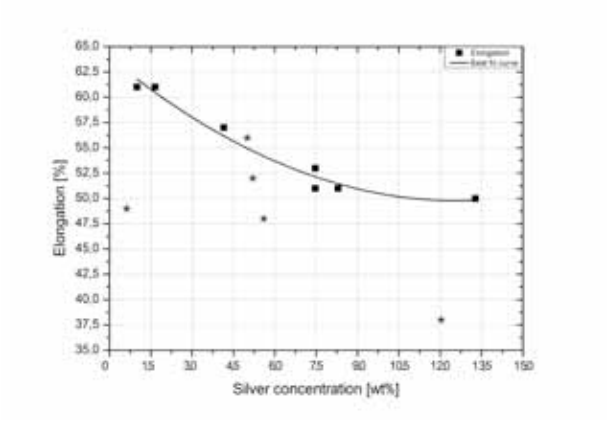

Figure 24 Graph of percent elongation to rupture against silver concentration (wt.%)

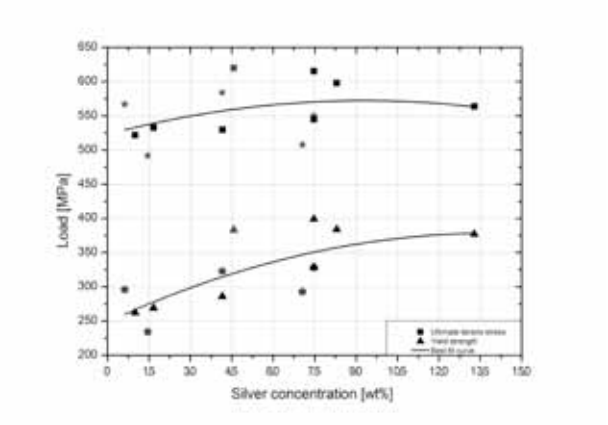

Figure 25 Graph of UTS and YS against silver concentration (wt.%)

Wrought 14K Red-Gold Alloys

Thirteen 14K red-gold alloys were suitable for plastic deformation (alloys 1, 3, 4, 5, 6, 7, 8, 12, 13, 14, 15, 16 and 18). In this case alloys with at least one grain refiner (either 1 or 2) were deemed suitable for deformation. We observed mechanical properties, drawability and work hardening of plastic deformation alloys. We used stars and pentagons to mark alloys with grain refiner 2 (alloys 1, 4, 6, 12, 13). The resulting trends were determined considering all alloys regardless of whether they featured grain refiner 1 or 2.

Generally speaking, Figure 25 shows that plastic deformation alloys have greater mechanical properties than investment casting alloys. Yield strength appears to increase with high silver concentration whereas UTS appears to have smaller increases. Truthfully, we did not achieve as clear a trend as we did with investment casting alloys. Rather, we found a wide range of values in the data that did not allow linking physical properties to chemical composition.

Figure 26 shows the graph on elongation based on silver concentration. In this case, as well, stars indicate alloys with grain refiner 2 and squares alloys with grain refiner 1. As with mechanical properties, it is not possible to correlate the resulting data with the variation of silver concentration and or with the type of grain refiner present.

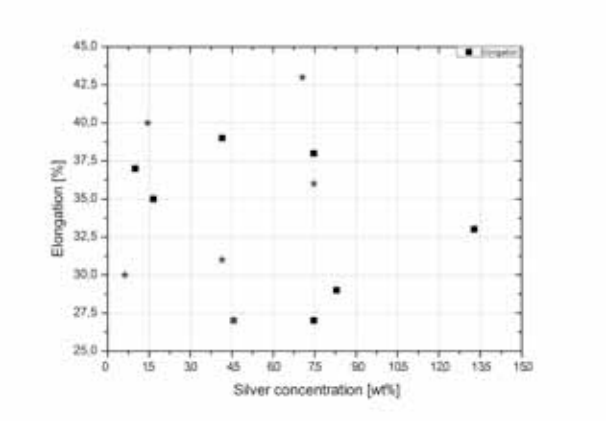

Figure 26 Graph of percent elongation to rupture against silver concentration (wt.%)

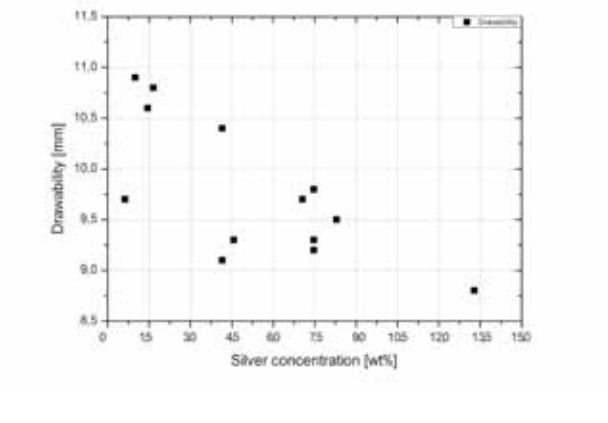

Figure 27 Graph of drawability against silver concentration (wt.%)

Moving on to analyzing general drawability, it should be noted that by increasing silver concentration drawability decreases. A clear trend cannot be set,this depending also on the fact that drawability is influenced by several factors as we have repeatedly highlighted, i.e., zinc concentration and grain size. For this reason we drew the graph in Figure 28 to show the trend of drawability for only those alloys containing grain refiner 1.
Considering that this is all experimental data, we

can affirm that alloys with grain refiner 1 (which feature a very close crystalline structure) tend to decrease in drawability when silver concentration increases, as is clearly shown in Figure 28 (the farthest value from the calculated trend is that of alloy 8, the alloy with the most zinc content but at the same time the one with the smallest grain size). Divergence can be imputed to different zinc content in different alloys.

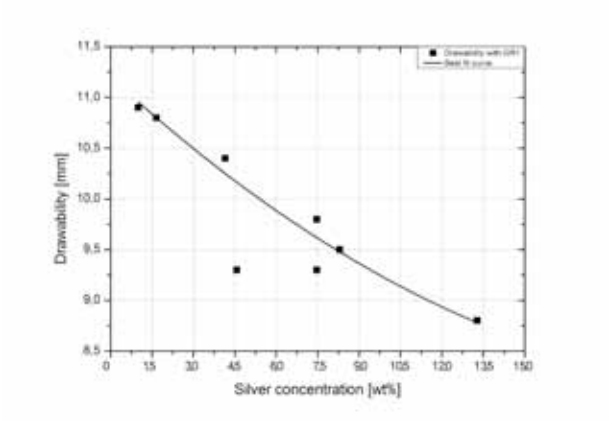

Figure 28 Graph of drawability of alloys with GR1 against silver concentration (wt.%)

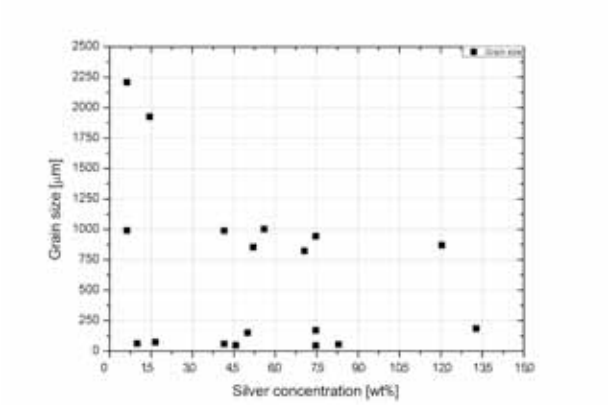

Figure 29 Grain of average grain size against silver concentration (wt.%)

As far as the size of crystalline grain is concerned (Figure 29), the same considerations stated for 14K yellow gold apply. Basically, alloys containing grain refiner 1 are well refined, excluding alloy 10, which in addition to grain refiner 1 also features a deoxidizer that tends to increase the size of the grain. Please note that alloy 9 has a grain refiner and a deoxidizer but features fine grain because the content of grain refiner in alloy 10 is much lower than in all the other alloys with grain refiner 1. After casting, grain refiner 2 does not appear to work any longer, whereas alloys with deoxidizer feature the largest grain possible. Our experience confirmed what we were expecting from a theoretical point of view.

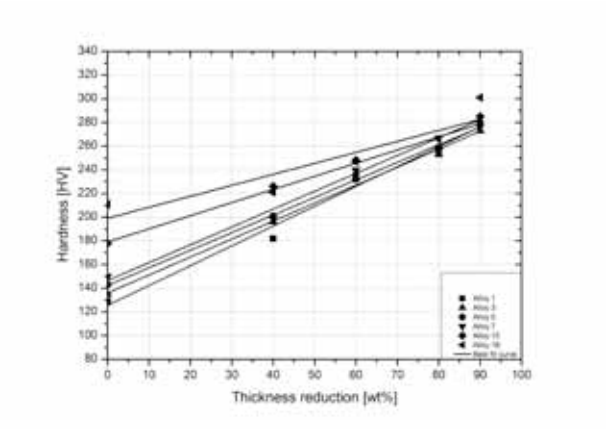

Figure 30 Work hardening best-fit curves for 14K red-gold alloys

Work-hardening curves highlight how increasing silver content in the alloy increases hardness, in accordance with trends observed for hardness in the graph in Figure 22. In this case, as well, we have drawn the curves of only some alloys (1, 3, 5, 7, 15, 18) to better appreciate their trend.

14K White-Gold Alloys

Seventeen white-gold alloys were analyzed, as seen in Table 3. These alloys were sorted in increasing order depending on nickel and zinc concentration.

Table 3 Composition of the investigated 14K white-gold alloys (weight %)

Specimen	Au	Ni	Zn	Ag	Cu	GR1	GR2	Deoxidizer
Alloy 1	585	41.5	41.5		Balance		X	
Alloy 2	585	41.5	62.25		Balance	X		X
Alloy 3	585	49.8	83		Balance			X
Alloy 4	585	62.25	41.5	62.25	Balance			X
Alloy 5	585	62.25	62.25		Balance		X	
Alloy 6	585	62.25	62.25	62.25	Balance			X
Alloy 7	585	62.25	103.75		Balance			X
Alloy 8	585	62.26	33.2	41.5	Balance	X		
Alloy 9	585	62.363	62.25		Balance	X		X
Alloy 10	585	62.454	58.1		Balance	X		
Alloy 11	585	62.505	58.1		Balance	X		X
Alloy 12	585	80	70	30	Balance	X		X
Alloy 13	585	83	49.8		Balance		X	
Alloy 14	585	83	74.7		Balance			X
Alloy 15	585	83.204	58.1		Balance	X		
Alloy 16	585	83.255	58.1		Balance	X		X
Alloy 17	585	84.594	74.7		Balance	X		X

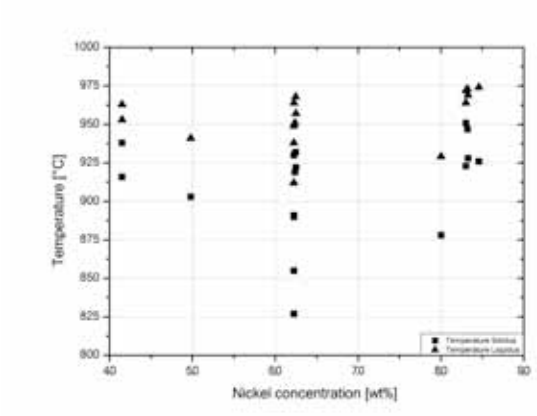

Figure 31 Graph of liquidus and solidus temperatures (°C) against nickel concentration (wt.%)

After analyzing all available data, it is not possible to extract a trend on solidus and liquidus temperatures. However, it should be noted that these alloys feature very different compositions. More specifically, we have to consider that all the compositions contain a different amount of zinc, even though they are nickel-based alloys with silver. This does not allow us to carry out specific observations on melting range based on data in Figure 31. For example, for alloys 4, 6, 8 and 12, silver tends to decrease solidus temperature and decrease the liquidus temperature even less, thereby increasing melting range compared to a silver-free alloy. Zinc content being equal, liquidus temperature tends to increase when nickel concentration increases (alloys 2, 5, 10, 15 where the zinc content is slightly different). Nickel concentration being equal, solidus temperature tends to decrease more than liquidus temperature when zinc content increases, thereby increasing melting range (a less marked phenomenon than the one observed with silver, i.e., alloys 1, 2, 5, 7, 10, 13, and 14).

Density analysis suffers as well from very different compositions. We can exclude the four alloys with silver, which obviously feature higher density than other alloys, and the resulting data is indicated with triangles in the graph in Figure 32. We believe density value can be considered constant when nickel content changes.

Basically, the graph shows there is a maximum density variation between the different silver-free alloys of less than 0.2g/cm3 (a value slightly greater than the limits of our measurement method). This, together with different zinc-content alloys, leads us to consider density constant when nickel concentration changes. For the same reason, the contribution of zinc to density variation is negligible.

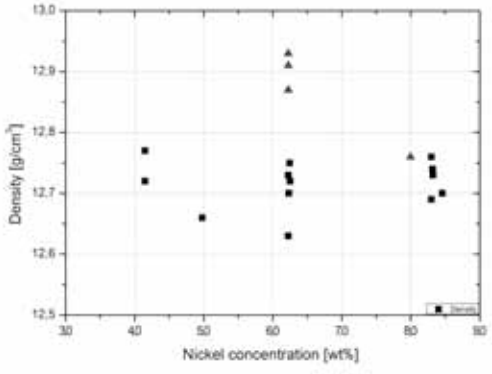

Figure 32 Graph of the density (g/cm³) against nickel concentration (wt.%)

With reference to L*, a* and b* coordinate trends, we plotted graphs in Figures 33, 34, 35 and 36. No trend depending on nickel can be found for L* coordinate. It appears L* is influenced by the con-

tent of zinc, but also by analyzing L* data based on zinc concentration, no acceptable trend can be found. We tried to check whether there was a correlation between L* and the sum of nickel and zinc (and also of nickel and double zinc), but with no result. We decided not to add these last two graphs because they are not significant. We can only say that, nickel being equal, L* seems to increase when zinc increases. Alloys with silver are indicated by stars.

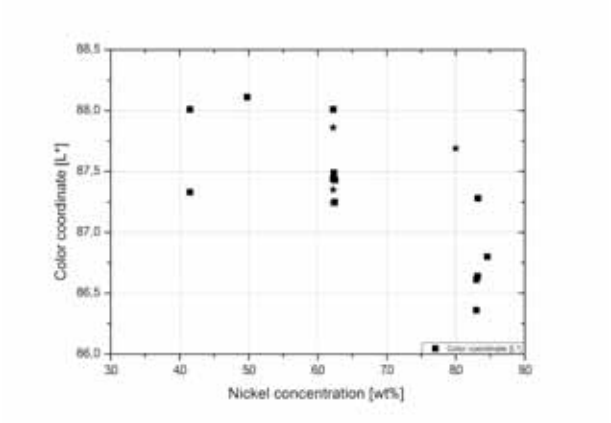

Figure 33 Graph of L* against nickel concentration (wt.%)

With reference to a* coordinate in Figure 34, it appears that it decreases when nickel increases. It is evident that a* is influenced also by zinc concentration so we decided to analyze the trend depending on nickel concentration added to zinc concentration, which would be the same as considering the content of copper. We used stars to indicate alloys with silver, which we did not consider in the interpolation in Figure 35. It is evident that when the sum of nickel and zinc increases, the hue of a* tends to shift towards green (to be more precise, it tends to be less red).

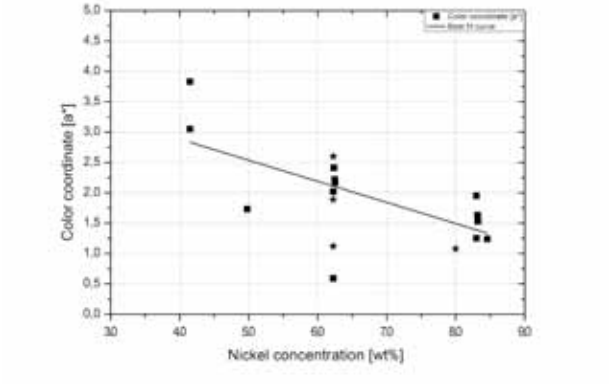

Figure 34 Graph of a* against nickel concentration (wt.%)

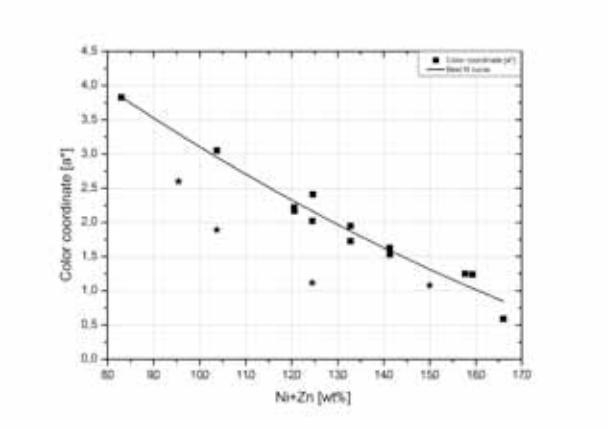

Figure 35 Graph of a* against nickel and zinc concentration (wt.%)

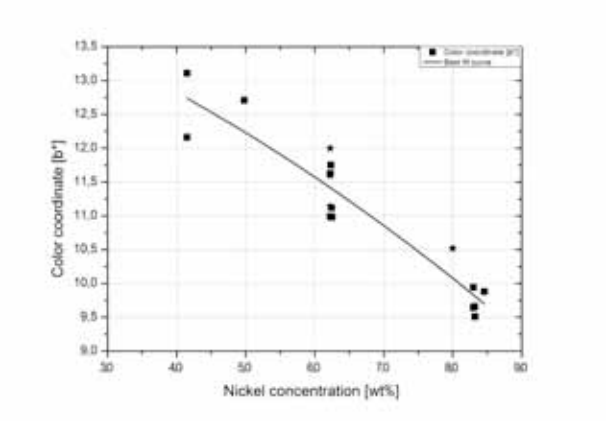

Figure 36 Graph of b* against nickel concentration (wt.%)

On the contrary, the b* value displays a certain trend dependent on nickel concentration (b* decreases when nickel concentration increases). As was found for L*, it is probable that zinc concentration influenced b* even though no trend can be found either by analyzing data based on the sum of nickel and zinc or in the sum of nickel and double zinc (the last two graphs are not shown because they are not typical).

As for colored gold, we analyzed the hardness trend after solution annealing and precipitation hardening (Figure 37). It should be noted that in general hardness tends to increase when nickel content increases. It is also clear why few alloys can be hardened. We believe we should consider only alloys 4 and 6 as hardenable because of 6.225% silver content. The other two alloys with silver (alloys 8 and 12) cannot be considered hardenable because hardness difference following precipitation hardening is less than 20% with alloy 8 and less than 10% with alloy 12 (compared to solution-annealed specimens). No other alloy displays hardening increases after hardening treatment. We believe the hardening mechanism is the same one as in colored gold (silver-based). The minor quantity of silver needed in the case of white gold is linked to the different starting

composition (the latter being nickel-based alloys). Even with 14K white gold, hardness is exclusively due to precipitation of a second silver-rich phase.

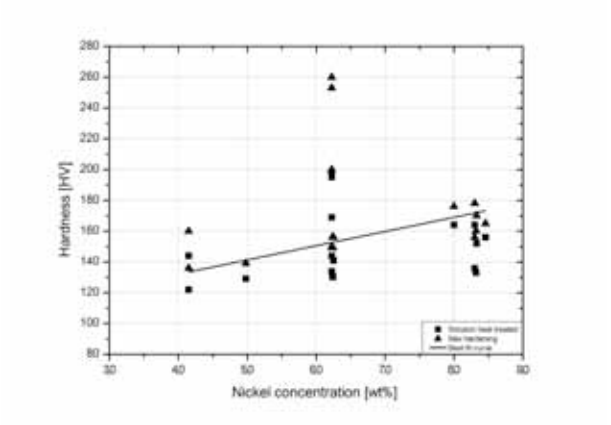

Figure 37 Graph of hardness against nickel concentration (wt.%)

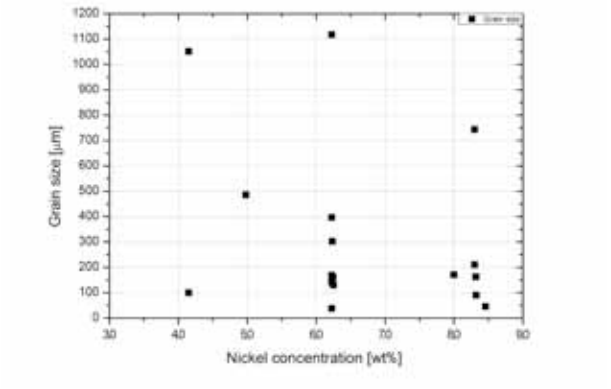

Figure 38 Graph of average grain size against nickel concentration (wt.%)

With reference to grain size, alloys with larger grains are the ones with the deoxidizer only. Alloys with grain refiner 2 also feature noticeably larger grains compared to alloys with grain refiner 1. When grain refiner 1 is used together with the deoxidizer, grains are comparable (same magnitude when talking about size) to the grains of alloys with grain refiner 1. Contrary to 18K, no decrease in grain size was observed when nickel and deoxidizer increased. We believe that in the case of 14K, the deoxidizer is solely responsible for grain size growth.

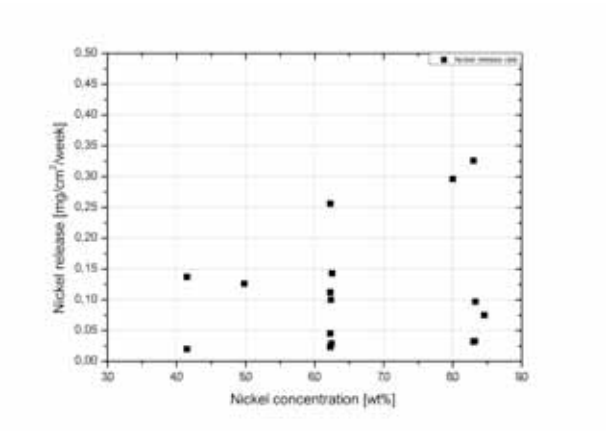

Figure 39 Graph of nickel-release rate against nickel concentration (wt.%)

The graph in Figure 39 is about nickel-release rate. As for 18K white gold, deoxidizers greatly foster the rate of nickel release. The alloys with higher release rates contain deoxidizers. Alloys with grain refiner show lower release values, composition being equal, thereby confirming the positive effect of grain refining on nickel release. Adding silver does not appear to have any real effect on release values (with the exception of alloy 8, the only one with silver but no deoxidizer). It could be assumed that the negative effect of deoxidizers is greater than the positive effect of silver (in 18K we did observe that silver reduced nickel-release rate). We can confirm that in this case nickel-release rate depends on nickel concentration but not exclusively.

14K White-Gold Alloys for Investment Casting

Eleven 14K alloys were suitable for investment casting (alloys 2, 3, 4, 6, 7, 9, 11, 12, 14, 16, and 17). We only considered alloys with at least one deoxidizer (grain refiner 1 may or may not be present).
With reference to UTS and yield strength, it can be generally affirmed that they both increase when nickel increases (Figure 40). We would like to emphasize that the four alloys with silver (represented by a star in the graph) tend to have UTS and yield strengths greater than the hypothetically silver-free alloy (with the same main composition). These alloys were not taken into consideration in the best fit plotted in the graph. A comparison of values shows that alloys with grain refiner show UTS and yield strengths greater than alloys with the deoxidizer only.

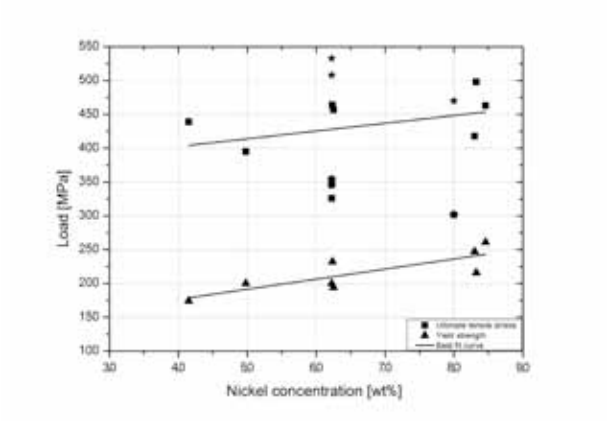

Figure 40 Graph of UTS and YS against nickel concentration (wt.%)

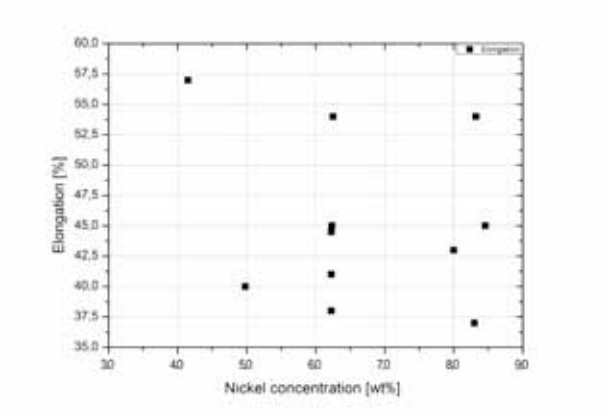

Figure 41 Graph of percent elongation to rupture against nickel concentration (wt.%)

It is not possible to draw an unequivocal trend in Figure 41 after casting deformation. It should be noted that alloys with only the deoxidizer show the most reduced elongation after casting. Nickel increase is followed by the tendency to reduce elongation. Silver, on the other hand, does not really seem to influence elongation.

Wrought 14K White-Gold Alloys

Eleven 14K alloys were suitable for plastic deformation (alloys 1, 2, 5, 8, 10, 11, 12, 13, 15, 16, and 17). In this case alloys with at least one grain refiner (and the likelihood of having at the same time a deoxidizer) were considered suitable for deformation. For plastic deformation alloys we recorded drawability and work-hardening curves in addition to mechanical properties. It appears that UTS and yield strength following annealing increase when nickel content increases, as with casting alloys. A behavior strictly dependent on the addition of grain refiner or deoxidizer elements can be observed. More specifically, there seems to be a great difference between alloys with both grain refiner and deoxidizer, which show greater UTS and yield strengths, and alloys with only grain refiner, as can be seen in Figure 42. Investment casting alloys with silver have superior mechanical properties. Silver therefore seems to increase mechanical properties of nickel white-gold alloys. In this case, as well, alloys with silver are represented in the graph with stars and pentagons.

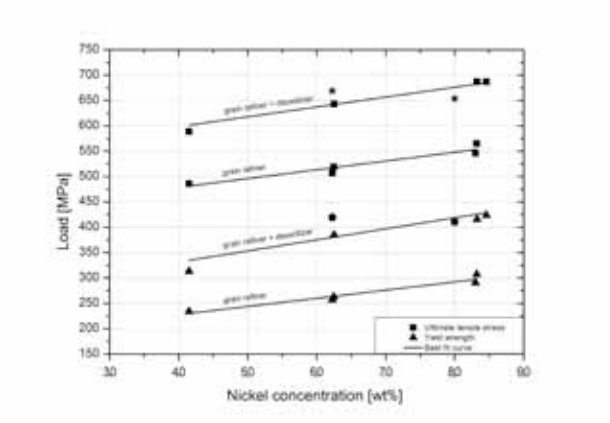

Figure 42 Graph of UTS and YS against nickel concentration (wt.%)

Elongation following annealing (Figure 43) shows the same trend as observed in the previous graph, i.e., alloys with grain refiner only (regardless of whether it is grain refiner 1 or 2) display greater elongation compared to alloys with grain refiner and deoxidizer. The elongation trend between the two groups tends to decrease when nickel content increases. Composition being equal, alloys with only grain refiner 2 display slightly greater elongation compared to alloys with only grain refiner 1.

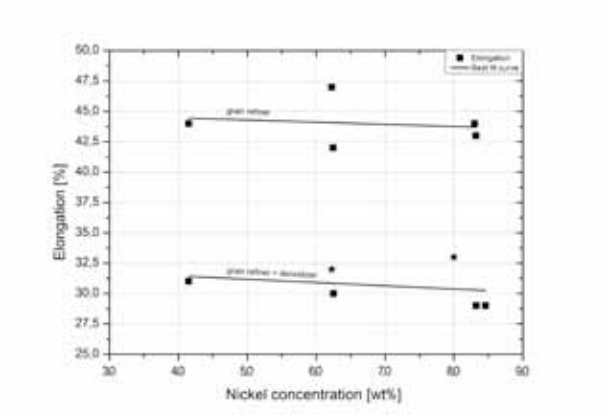

Figure 43 Graph of percent elongation to rupture against nickel concentration (wt.%)

The Erichsen test results, in our opinion, confirm what we already saw with tensile test data. Alloys with highest drawability values feature a grain refiner (either grain refiner 1 or 2), whereas alloys with grain refiner and deoxidizer display lower values. Drawability tends to decrease when nickel content increases. Alloys with silver display lower Erichsen test values, which are indicated in the graph in Figure 44 with a star.

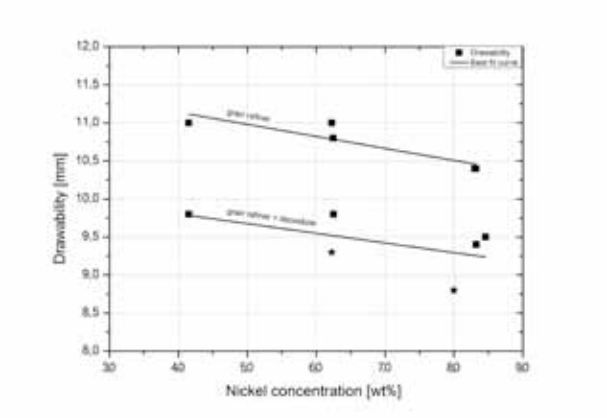

Figure 44 Graph of drawability against nickel concentration (wt.%)

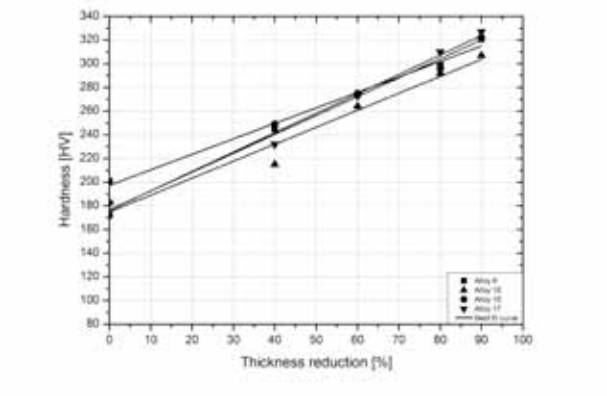

Figure 45 Work-hardening best-fit curves for 14K white-gold alloys

Work-hardening curves display the same trend as for 18K, i.e., when nickel increases the material tends to work harden more. The graph in Figure 45 features alloys 8, 10, 15, and 17.

Conclusions

As anticipated last year, we focused this paper on 14K alloys. We can confirm that the data collected basically reflect what our daily experience tells us. Clearly there are a few results that departed from the expected trend. We have to analyze if they could depend on the experimental conditions. To do that, we should characterize tailor-made alloys in order to observe the accuracy of trends. It appears we must carry out more tests on white gold because, in many cases, we did not find correlations between the different compositions. Nonetheless, because of the information now at our disposal, we believe the data enable us to choose the best composition for the use required.

References

"Properties and Selection: Non ferrous Alloys and Special-Purpose Materials,"*ASM Handbook 2.*

Dieter Ott, "Influence of Small Additions and Impurities on Gold and Jewerly Gold Alloys," *The Santa Fe Symposium on Jewerly Manufacturing Technology 1997*, ed. Dave Schneller (LaFayette, CO: MetChem Research, 1997): 173-196.

A. S. McDonald and G. H. Sistare, "The Metallurgy of Some Carat Gold Jewellery Alloys," *Gold Bulletin 11*, no. 3 (1978): 66-73.

W. S. Rapson, "The Metallurgy of the Coloured Carat Gold Alloys," *Gold Bulletin 23*, no. 4 (1990): 125-133.

W. S. Rapson and T. Groenewald, *Gold Usage* (Academic Press, 1978).

L.S. Benner, T. Suzuki, K. Meguro and S. Tanaka, *Precious Metals and Technology* (International Precious Metals Institute).